Pioneer. Adv. Mater. 2026, 2(1): 1-15 DOI: 10.48308/piadm.2026.245206.1027

Shahid Beheshti University

Pioneering Advances in Materials

Journal homepage: http://piadm.sbu.ac.ir ISSN: 3115-7114

Research paper

The Investigation of Permanent Magnetic Waveguide Lattice in Presence of 3D Bias Magnetic Field Components

Parvin Karimi*

Department of Physics, ST.C., Islamic Azad University, Tehran, Iran

*p.karimi@iau.ac.ir

Article info:

Article history:

Received: 03/07/2026

Accepted: 21/08/2026

Keywords:

Magnetic lattice, Atom chip, Ultracold atoms, Magnetic microtraps, Permanent magnet films

Abstract

In this paper, we propose a permanent magnetic waveguide lattice produced by high quality magneto-optical film FePt for confining, controlling and manipulating ultracold atoms, quantum degenerate gases, and Bose–Einstein condensates (BECs). We also consider the components of an external bias magnetic field B_{1x}, B_{1y} and B_{1z} to provide further control over the parameters of magnetic lattice. For the first time, we derive analytical expressions describing the dependence of the trap parameters, including the locations of the magnetic field minima, the curvatures of the absolute value of the magnetic field, trap frequencies, magnetic field barrier heights, and trap depths, on the value of external bias magnetic fields along the *x*, *y*, and *z* directions. Furthermore, numerical calculations are carried out for a magnetic lattice size $n_s = 71$ and the corresponding results are compared for two cases $B_{1z} = 0$ and $B_{1z} \neq 0$. The results demonstrate that considering $B_{1z} \neq 0$ leads to deeper trapping potentials compared with the case of $B_{1z} = 0$.

1. Introduction

Atom chips are complex microstructures that can generate flexible trapping potentials with arbitrary geometries including single trap and periodic array of traps in various lattice platforms [1]. The realization of Bose–Einstein condensates (BECs) in these structures [2, 3] has motivated numerous research groups to investigate the fundamental properties and behavior of ultracold atoms on atom chips [4-7]. In this regard, optical lattices were introduced as a powerful tool for controlling ultracold atoms. These periodic potentials are generated by the interference of counter-propagating laser beams in different dimensions [8, 9]. These structures provide suitable configurations for trapping, confining, controlling and manipulating ultracold atoms and BECs [8, 10]. They have enabled various theoretical and experimental investigations including quantum simulations [11], quantum physics experiments at low temperatures [9], quantum phase transition from superfluid to Mott insulator [12], and quantum computation [13]. To date, various applications of optical lattices have been reported, such as the creation of artificial crystals for studying condensed matter theories [14] and the development of optical lattice clocks [15]. A complementary alternative to optical lattices is provided by magnetic lattices which can be fabricated using current-carrying wires [16-18] and permanent magnetic lattices produced by high quality magneto-optical films [19-21]. These arrays provide stable trapping configurations for confining ultracold atoms [22]. One of the important features of magnetic lattices is flexibility in design and fabrication, which allows arbitrary geometries to be realized [19-21, 23, 24]. The first type of magnetic lattice is a magnetic waveguide array, which can be fabricated using current-carrying wires or permanent magnetic slabs to generate two-dimensional traps [19]. Furthermore, several types of two-dimensional periodic permanent magnetic arrays capable of generating three-dimensional traps have been studied and analyzed, including two crossed layers of parallel rectangular magnets [19], a two-dimensional array of square magnetic slabs [20], a two-dimensional lattice of square holes [21], a single layer of periodic arrays of square magnets with different thicknesses [20], and two crossed periodic arrays of parallel rectangular magnets at an arbitrary angle [19] .Recently, a 3D permanent magnetic lattice has been introduced, consisting of separated layers of 2D arrays that can generate trapping potentials with higher trap frequencies than those of a single-layer configuration [24]. In general, several significant features have established permanent magnetic lattices as promising alternatives to optical lattices and current-carrying wires [23, 24]. First, the atom loss in current-carrying wires can occur due to increased heating rates and current densities, whereas this effect is not observed in permanent magnetic lattices fabricated from high-quality magneto-optical films. Second, unlike optical lattices, these structures do not require laser beams for trapping ultracold atoms in magnetic microtraps, and they are not affected by fluctuations in the laser beams. Third, in these structures, decoherence due to spontaneous emission is significantly reduced. Fourth, permanent magnetic lattices provide large curvatures of magnetic field, resulting in stable, deep, and controllable trapping potentials with high trap frequencies. Fifth, in these configurations, ultracold atoms are trapped in the low magnetic field-seeking states, thereby significantly reducing atom loss caused by Majorana spin-flip transitions and enabling more efficient evaporative cooling [19, 24]. In general, the properties of ultracold atoms in permanent magnetic lattices are investigated through both analytical expressions and numerical calculations. Therefore, the trap parameters such as the non-zero magnetic field minima, the location of the magnetic field minima, the curvatures of the magnetic field, trap frequencies, and trap depths can be adjusted by varying the external bias magnetic field components [19-21, 23, 25]. To date, permanent magnetic lattices have been the subject of theoretical and experimental investigations. For example, the use of radio frequency spectroscopy for the measurement of the Bose-Einstein condensate in a 1D magnetic lattice has been reported in Ref. [26]. In addition, Singh et al. [27] have reported experimental observations of the reflection of ultracold atoms from a 1D magnetic lattice. Moreover, a numerical algorithm has been employed to generate the desired Ioffe-Pritchard magnetic lattice configurations for trapping ultracold atoms [28]. In another study, the trapping of ultracold ^{87}Rb atoms at a distance of approximately 100 nm above a sub-micron triangular structure atom chip consisting of several Co/Pd layers has been shown

[29]. A two-dimensional tooth-shaped permanent magnetic lattice has been proposed to produce Ioffe-Pritchard potentials and control ultracold atoms using analytical calculations [25]. Furthermore, Ref. [30] has demonstrated that ultracold atoms can be trapped in a magnetic lattice fabricated from a thin FePt film as a platform for quantum experiments. Moreover, the quantum phase transition from superfluid to Mott insulator the can be simulated and the critical point can be determined [31, 32]. Recently, the application of Artificial Intelligence (AI) to quantum phase transitions, ultracold atoms, and optical and magnetic lattices has been reported in several studies [33-36]. In this paper, we propose a permanent magnetic waveguide lattice produced by high quality magneto-optical film FePt in the presence of three components of the external bias magnetic field (B_{1x}, B_{1y}, B_{1z}) to investigate enhanced control of ^{87}Rb atoms in the low magnetic field-seeking state $|F=+2, m_F=+2\rangle$. For the first time, we derive analytical expressions describing the dependence of the trap parameters including the locations of the magnetic field minima, the curvatures of the absolute value of the magnetic field, trap frequencies, the magnetic field barrier heights, and trap depths on the external bias magnetic fields along the *x*, *y*, and *z* directions.

It is shown that the expressions reported in Ref. [19] are obtained by considering $B_{1z}=0$. Also, we compare the analytical results for two cases, $B_{1z}=0$ and $B_{1z}\neq 0$, to investigate the effect of this bias magnetic field component on the trap parameters. Moreover, we perform numerical calculations for a finite lattice size with $n_s=71$, plus the edge-compensation analysis based on the compensation method reported in previous studies [21]. We show that, in the case $B_{1z}\neq 0$, the values of both the trap frequencies and the trap depths are enhanced, which enables improved control of magnetic microtraps.

2. 1D permanent magnetic waveguide lattice

Figure (1) shows a permanent magnetic waveguide lattice produced by high quality magneto-optical film FePt. It consists of an infinite array of long, parallel rectangular magnets with thickness *t*, periodicity *a* along the *x* direction and magnetization M_z oriented in the direction opposite to the *z*-axis, in the presence of external bias magnetic field components (B_{1x}, B_{1y}, B_{1z}). The components of the magnetic field are given by

$$B_x = B_{1x} \tag{1a}$$

$$B_y = B_{0y}\,sin(ky)e^{-kz} + B_{1y} \tag{1b}$$

$$B_z = B_{0y}\,cos(ky)e^{-kz} + B_{1z} \tag{1c}$$

where $B_{0y} = B_0(1-e^{-kt})e^{kt}, B_0 = 4M_z$ and $k=\frac{2\pi}{a}$. Also, the magnitude of the magnetic field is

$$B = \{B_{1x}^2 + B_{1y}^2 + B_{1z}^2$$
$$+2B_{0y}[B_{1y}\,sin(ky) + B_{1z}\,cos(ky)]e^{-kz} \tag{2}$$
$$+B_{0y}^2 e^{-2kz}\}^{1/2}$$

The analytical Eqs. (3a) and (3b) show the coordinate of the magnetic field minima $(y_{\min}, z_{\min})$

$$y_{min} = a(n_y + \frac{1}{2\pi}tan^{-1}(\frac{|B_{1y}|}{|B_{1z}|})) \tag{3a}$$
$$n_y = 0, \pm 1, \pm 2, \ldots$$

$$z_{\min} = \frac{1}{k}Ln\left(\frac{B_{0y}}{\left(B_{1y}^2 + B_{1z}^2\right)^{1/2}}\right) \tag{3b}$$

Moreover, we have the magnetic field minima based on (2), (3a) and (3b)

$$B_{min} = |B_{1x}| \tag{4}$$

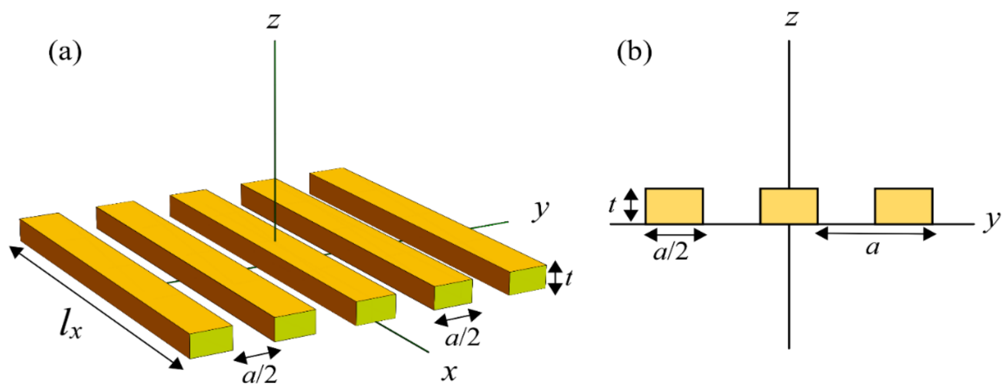

Figure 1. (a) 3D plot of an infinite periodic array of long, parallel rectangular magnets (b) 2D plot in the *y-z* plane , showing the thickness *t* and periodicity *a*

Also, the curvatures of the magnetic field at the trap centers are obtained

$$\frac{\partial^2 \mathrm{B}}{\partial \mathrm{x}^2}=0 \tag{5}$$

$$\frac{\partial^2 \mathrm{B}}{\partial \mathrm{y}^2}=\frac{\partial^2 \mathrm{B}}{\partial \mathrm{z}^2}=\frac{k^2\left(B_{1z}^2+B_{1y}^2\right)}{|B_{1x}|} \tag{6}$$

Using the Eqs. (5) and (6), the trap frequencies are defined

$$\omega_i=\left(\frac{m_F g_F \mu_B}{m}\frac{\partial^2 B}{\partial x_i{}^2}\right)^{1/2} \qquad i=2,3 \tag{7}$$

In this expression, m_F, g_F, μ_B, and m are the magnetic quantum number of hyperfine state F, the Land´e g-factor, the Bohr magneton, and the atomic mass of ^{87}Rb in low magnetic field-seeking state $F=+2$ and $m_F=+2$ respectively. Another important parameter that can be calculated is the magnetic field barrier heights along the *y* and *z* directions

$$\Delta B^y=\sqrt{B_{1x}^2+4\left(B_{1y}^2+B_{1z}^2\right)}-B_{\min} \tag{8}$$

$$\Delta B^z=\sqrt{B_{1x}^2+B_{1y}^2+B_{1z}^2}-B_{\min} \tag{9}$$

Based on this parameter, the trap depths along the different directions can be given by

$$\Delta U^{(x_i)}=U_{\max}^{(x_i)}-U_{\min} = m_F\mu_B g_F \Delta B^{(x_i)} \qquad i=2,3 \tag{10}$$

Based on the Eqs. (3a)-(9), two main calculations can be drawn. First, all analytical expressions depend on the external bias magnetic field components particularly in the *z* direction excepted for the magnetic field minima. Second, by setting $B_{1z}=0$, all equations reduce to the results reported in Ref [19]. It is found that increasing the B_{1z}component leads to higher values of the trap frequencies and the trap depths.

3. Results and discussions

To present a comprehensive study, we discuss results using two approaches, analytical and numerical, based on Eqs. (3a)-(10), the Radia package interfaced with Mathematica, and the input parameters listed in Tables (1) and (2) for two cases $B_{1z}\neq 0$ and $B_{1z}=0$ followed by a comparison of the results.

3.1. Analytical results

Figures 2(a)-(b) show the location of the magnetic field minima $\vec{r}_{\min}=(y_{\min},z_{\min})$ given by Eqs. (3a) and (3b) as a function of B_{1z} using constant values in Table (1) for two cases $B_{1z}\neq 0$ and

$B_{1z} = 0$ by comparison their values. It can be seen that as $|B_{1z}|$ approaches zero, y_{min} and z_{min} increase, and the corresponding values of $y_{\min} = 0.250\ \mu m$ and $z_{\min} = 1.212\ \mu m$ become accessible for $B_{1z} = 0$.

Figures 3(a) and 3(b) present the variations of the trap frequencies along the y and z directions as a function of B_{1x} and B_{1y} for two cases $B_{1z} = 0$ and $B_{1z} \neq 0$. As shown in Figure 3(a), for $B_{1y} = -4.000\ (G)$ and $B_{1z} = -8.000\ (G)$, increasing $|B_{1x}|$ leads to reduction in both ω_y and ω_z. This behavior agrees well with the analytical expressions (6) and (7). Furthermore, for a given value of $|B_{1x}|$, the inclusion of the $B_{1z} \neq 0$ component results in higher trap frequencies compared with the case of $B_{1z} = 0$.

Moreover, Figure 3(b) demonstrates an opposite trend in the trap frequencies along the y and z directions as a function of $|B_{1y}|$ for the considered values of $B_{1x} = -2.000\ (G)$ and $B_{1z} = -8.000\ (G)$. Similarly, as shown in Figure 3(a), in the case of $B_{1z} \neq 0$ the values of ω_y, ω_z are higher than those in $B_{1z} = 0$ case at a given value of $|B_{1y}|$.

Table 1. Input parameters for waveguide lattice used in both analytical and numerical calculations

Parameter	Definition	Analytical	Numerical
n	Number of rectangular magnets along the x direction	∞	71
$a(\mu m)$	Period of magnetic lattice	1.000	1.000
$t(\mu m)$	Thickness of magnetic film	0.050	0.050
$4\pi M_z(G)$	Magnetization along the z direction	3800	3800

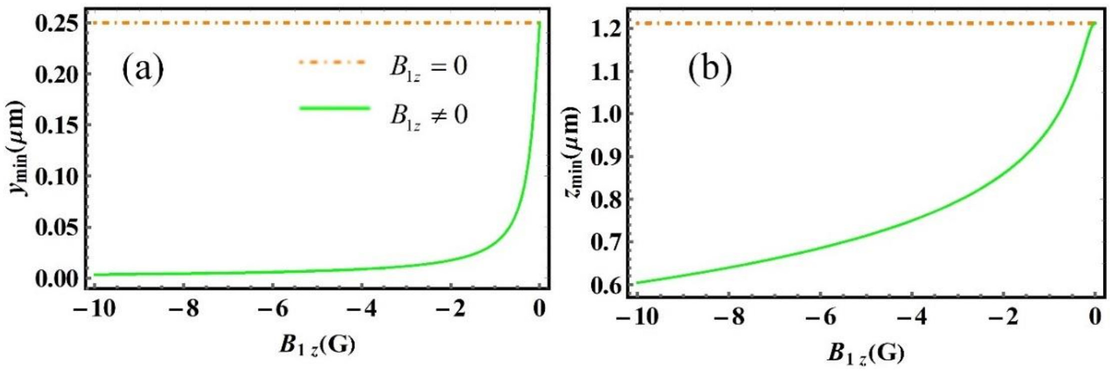

Figure 2. Variation of magnetic field minima location $\vec{r}_{\min} = (y_{\min}, z_{\min})$ as a function of B_{1z} (a) y_{min} (b) z_{min} using the constant values listed in Table (1) and $B_{1y} = -0.220$ (G)

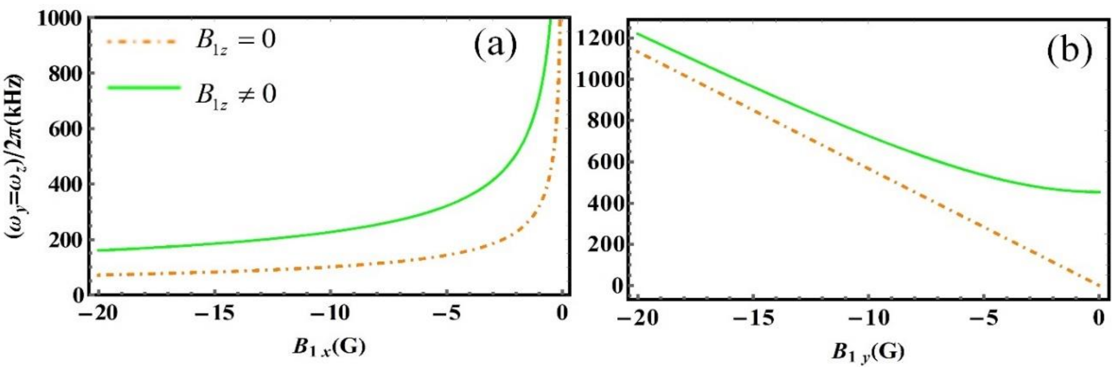

Figure 3. Comparison of trap frequencies along the y and z directions for two cases $B_{1z} = 0$ and $B_{1z} \neq 0$ (a) versus B_{1x} for constant values $B_{1y} = -4.000\ (G)$ and $B_{1z} = -8.000\ (G)$ (b) as a function of B_{1y} for fixed values $B_{1x} = -2.000\ (G)$ and $B_{1z} = -8.000\ (G)$

Another important parameter that can be obtained is the trap depths defined by Eqs. (8)-(10). Similar to trap frequencies, Figures 4(a)-(d) show the comparative changes of ΔU^y and ΔU^z as a function of B_{1x} and B_{1y} for two cases $B_{1z} = 0$ and $B_{1z} \neq 0$.

The analysis of Figures 4(a) and 4(b) indicates that the potential barrier height along the *y* direction exhibits higher values for the case $B_{1z} \neq 0$ compared with $B_{1z} = 0$ over different values of $|B_{1x}|$ and $|B_{1y}|$.

In addition, the same behaviors are observed in Figures 4(c) and 4(d) for ΔU^z. The variations shown in Figures 4(a) and 4(c) indicate that the increasing $|B_{1x}|$ leads to a decrease in ΔU^y and ΔU^z, while the opposite behavior is observed in Figures 4(b) and 4(d). Moreover, Figure (5) and Figures 6(a) and 6(b) show that the previously discussed parameters exhibit higher values with increasing B_{1z}.

These results agree well with the analytical expressions (6) to (10), indicating that the higher values of $|B_{1z}|$ enhance the trap frequencies and the trap depths.

Therefore, the analysis of Figures (3)-(6) shows that B_{1z} is an effective variable for the trap frequencies and potential barrier height that can provide more control over the trap and generate deeper permanent magnetic microtraps.

Figure (7) illustrates the analytical dependence of z_{min} on the thickness of the magnetic film (*t*) obtained from Eq. (3b).

It is clear that increasing *t* causes z_{min} to shift toward larger distances.

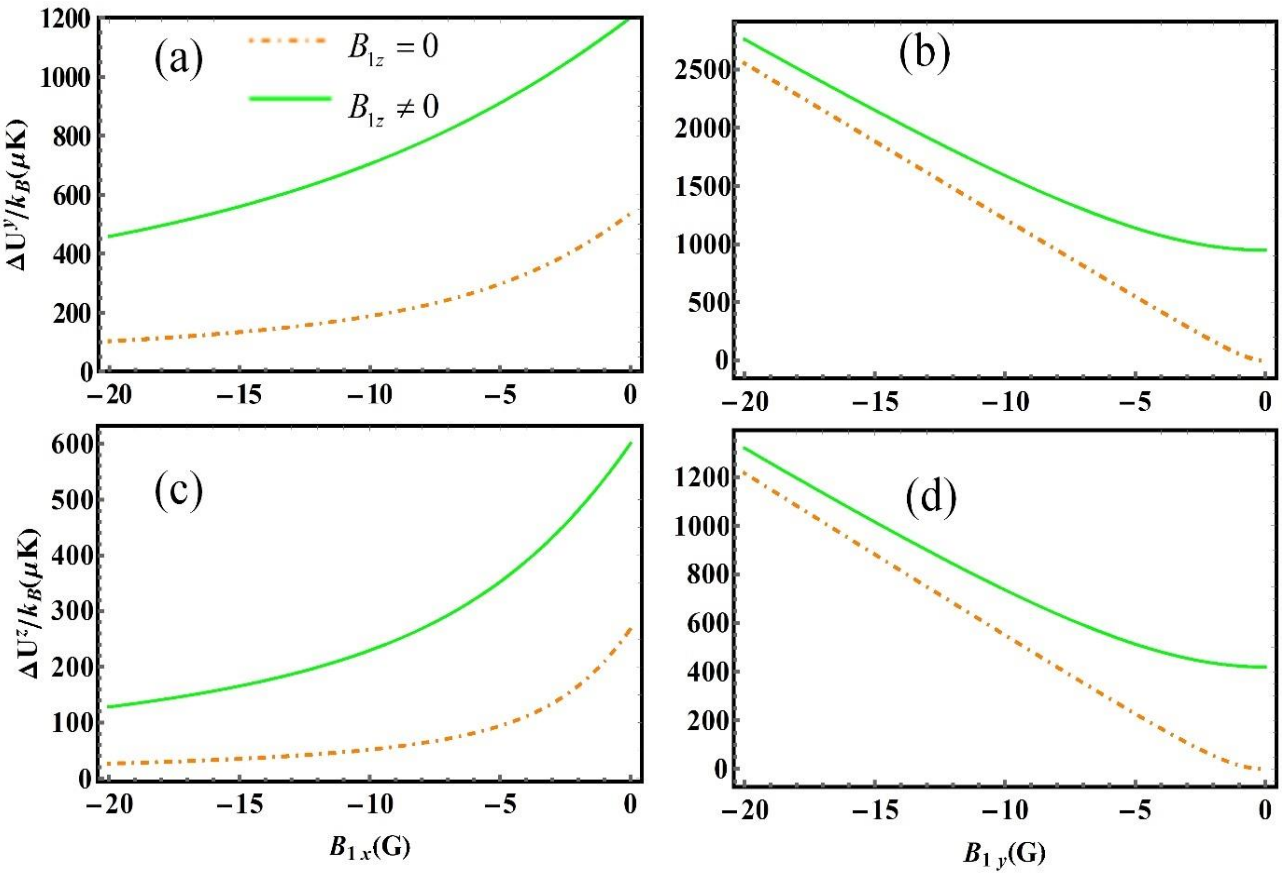

Figure 4. Variation of the potential barrier height in (a) the *y* direction and (c) the *z* direction as a function of B_{1x} for $B_{1y} = -4.000\ (G)$ and $B_{1z} = -8.000\ (G)$ in (b) the *y* direction and (d) the *z* direction versus B_{1y} for $B_{1x} = -2.000\ (G)$ and $B_{1z} = -8.000\ (G)$

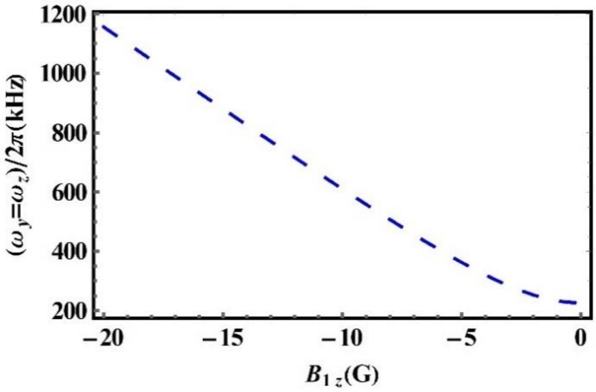

Figure 5. Variation of the trap frequencies along the y and z as a function of B_{1z}

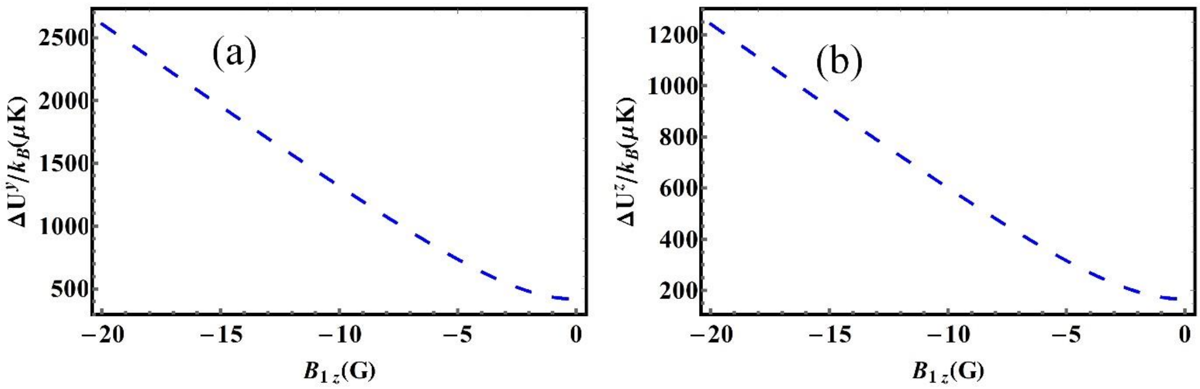

Figure 6. Dependence of the potential barrier height for the y and z directions on B_{1z}

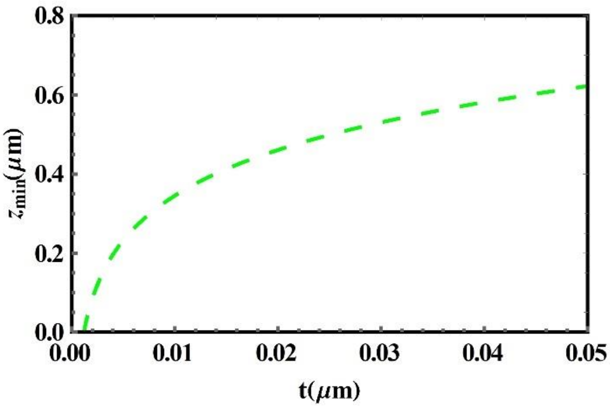

Figure 7. Variation of z_{min} with the magnetic film thickness t

3.2. Numerical results

To further investigate the obtained results, numerical calculations are performed using the Radia software package interfaced to Mathematica to validate and compare the analytical results. Unlike the analytical approach, which assumes an infinite lattice size, the numerical calculations are performed by considering a finite array of rectangular magnetic slabs for simulation. Therefore, the comparison between the analytical expressions and numerical calculations is reasonable when the edge (size) effect is considered. In fact, this parameter corresponds to a magnetic field component in the negative z direction that compensates for the missing contributions of the finite lattice from the edge of the structure to infinity. Here, the dimension of the permanent magnetic waveguide array is $n_s = 71$ and the edge effect for this finite lattice is $B_{1zc} = -1.212\ (G)$. Using the input parameters in Table (1) and the external bias magnetic field components along the x, y and z directions listed in Table (2) the analytical and the numerical results for various magnetic microtraps parameters are reported in Table (3). According to Refs. [1, 37], the choice of the external bias magnetic field components along the x and y directions reported in Table (2) is justified. The atoms remain confined in the traps without loss, provided that the trap depth satisfies the condition $UF_{F_B}B_{max_{max}}$ where $\eta = 5 - 7$. This condition is usually considered for the external bias magnetic field components in the x and y directions. Therefore, by considering $B_{1x} = -2.730$ G, $B_{1y} = -0.22$ G, $B_{1z} = 0$, $k_B T = 0.94 \times \hbar \times \bar{\omega} \times n^{1/3}$, and $\bar{\omega} = (\omega_y \omega_z)^{1/2}$, the ratios for $n = 3 \times 10^5$ atom are $U_{max\,y}/k_B T = 5.76$ and $U_{max\,z}/k_B T = 5.70$ Hence, the selected values of bias magnetic field components are reasonable. To show the effect of B_{1z} on the trap parameters, the third column in Table (3) presents the analytical results corresponding to $B_{1z} = 0$ as reported in Ref. [19].

It is obvious that, for $B_{1z} \neq 0$ the results presented in the fourth and fifth columns for the analytical and numerical approaches are in good agreement, and both exhibit higher values compared with the $B_{1z} = 0$ case.

This comparison confirms that B_{1z} is an important parameter for controlling of the magnetic lattice parameters, resulting in deeper traps and higher trap frequencies.

Figures 8(a) and 8(b) depict the comparison of the absolute value of the non-zero magnetic field, B, versus the y and z directions. To generate these plots, the analytical results obtained from Eq. (2) for an infinite lattice size are compared with the Radia simulation results for finite lattice size $n_s = 71$.

The analytical (solid line) and numerical (dashed line) results exhibit good agreement using the input parameters listed in Tables (1) and (2). Additionally, Figure 9(a) presents the 3D plot of non-zero magnetic field minima and Figures 9(b) and 9(c) display the contour plot of magnetic field B for $z = z_{min}$ and $y = y_{min}$ respectively. To further investigate the properties of the permanent magnetic waveguide array, different lattice sizes, including $n_s = 11, 21, 31, 41, 51, 101, 201, 301, 401, 501, 1001$ are considered to examine the variation of the compensating magnetic field component B_{1zc}, the magnetic field minima B_{min}, and the magnetic field minima location $\vec{r}_{\min} = (y_{\min}, z_{\min})$ with lattice sizes n_s. Figures 10 (a)-(d) show these trends.

As shown in Figure 10(a), increasing n_s causes the magnetic field minima B_{min} to approach $B_{\min} = 2.730$ (G). Moreover, Figure 10(b) indicates a gradual reduction in the compensating magnetic field component with increasing n_s; for example $B_{1zc} = -0.086\ (G)$ at $n_s = 1001$. These results clearly indicate two main consequences: first, as the number of rectangular magnetic slabs increases, the lattice size approaches that of an infinite lattice, and the compensating magnetic field component becomes negligible; second, the magnetic field minimum converges to the analytical results.

In contrast, Figures 10(c) and 10(d) show the opposite trends for y_{min} and z_{min}. Due to the increasing number of rectangular magnetic slabs, the value of y_{min} increases and becomes close to $y_{\min} = 0.250$ (μm).

Based on Figure 10(d), z_{min} exhibits the opposite behavior with respect to the variation of n_s, reaching $z_{\min} = 1.212$ (μm) at $n_s = 1001$. Table (4) presents the numerical results of Figures (10) for different parameters and lattice sizes using the input parameters listed in Tables (1) and (2).

Table 2. Specific values of the external bias magnetic field components along the *x*, *y* and *z* directions, as well as the edge effect for $n_s = 71$

Parameter	Definition	Analytical	Numerical
B_{1x} (G)	Bias magnetic field along the *x*	-2.730	-2.730
B_{1y} (G)	Bias magnetic field along the *y*	-0.220	-0.220
B_{1z} (G)	Bias magnetic field along the *z*	-4.000	-4.000
$B_{z(edge\ effect)}$	The compensating magnetic field component	0	-1.212

3.3. Experimental feasibility discussion

Since experimental investigation is not feasible, the physical effects arising in magneto-optical films and their influence on magnetic microtraps are theoretically estimated at $z_{\min} \approx 1.2\ \mu$m for $B_{1z} = 0$. These effects include the Casimir–Polder interaction, Johnson noise, corrugation from film inhomogeneity, and gravitational sag.
For the Casimir–Polder interaction, based on the reported data, $z_{\min} = 1.212\ \mu$m, $\Delta B^y = 0.035$ G, $\Delta B^z = 0.009$ G, $\Delta U^{x,y} = m_F \mu_B g_F \Delta B^{x,y}$, $m_F = 2$ and $g_F = 1/2$ for ^{87}Rb atom in the $|F = +2, m_F = +2\rangle$ state, are considered, and the corresponding values of ΔU^x=3.24×10^{-29}J and $\Delta U^y = 8.34 \times 10^{-30}$J are obtained. Casimir-Polder interaction is defined as $U_{CP} = -C_4/z^4$ [38]. For ^{87}Rb atoms near the FePt surface and the corresponding value $C_4 = 2.1 \times 10^{-55}$ J.m^4, the Casimir-Polder interaction is estimated as $|U_{CP}| = 9.732 \times 10^{-32}$. Consequently, the ratios $|U_{CP}|/\Delta U^x = 0.003$ and $|U_{CP}|/\Delta U^y = 0.011$ are obtained. Therefore, Casimir– Polder interaction energy does not significantly change trap confinement. Johnson noise is a detrimental mechanism for atom loss from a trap and is particularly relevant in the vicinity of conducting surfaces. In this region, thermally induced currents generate fluctuating magnetic fields that can induce spin flips in trapped atoms, causing transitions from low magnetic field-seeking to high magnetic field-seeking states and consequently leading to atom loss from the trap [39, 40]. For ^{87}Rb atoms near the FePt surface, by considering $t = 50$ nm, $z_{\min} = 1.212\ \mu$m, $T = 300$ K, $B_0 = 2.739$ G, and $\rho = 40 \times 10^{-7}\ \Omega$.m [41] the angular Larmor frequency $\omega_L = 1.204 \times 10^7$ rad/s and skin depth $\delta_L = \sqrt{2/\mu_0 \sigma \omega_L} \approx 230$ μm. Therefore, based on Eq. (4) in Ref. [40], we are in regime $t \ll z \ll \delta$ corresponding to the thin film. Hence, the Johnson spin-flip rate is $\Gamma_{Johnson} = 6.42 \times 10^{-2}$ s^{-1} and the Johnson-limited lifetime is $\tau_{Johnson} = 15.6$ s. The Johnson-noise-induced spin-flip rate is approximately $0.064 s^{-1}$, giving a characteristic timescale is approximately 16 seconds.

Thus, Johnson noise is not expected to cause rapid atom loss from the trap at the considered atom–surface distance. For corrugation from film inhomogeneity, a theoretical framework has been introduced in Ref. [42]. References [26, 27, 29, 30] are relevant studies on corrugation arising from film inhomogeneity; however, they do not provide a framework for calculating this effect directly .Whitlock et al [42] presented a theoretical method for estimating this effect and evaluating the influence of magnetization inhomogeneity on the trap depth. Based on this approach, the characteristic feature size of the domain structure, (*d*), is required.

However, this parameter, as well as the rms magnetization inhomogeneity (ΔM) parameter, has not been determined accurately for the FePt film considered here. Although, Ref. [30] investigates FePt magnetic films, it does not provide the specific information required for a quantitative application of the model. Therefore, a reliable quantitative estimate of the corrugation arising from film inhomogeneity in the FePt film cannot be obtained. Gravitational sag is defined as$\delta z = g/\omega^2$ [43]. For parameters $z_{\text{min}} = 1.212\ \mu\text{m}$ and $\omega_{trap} = 94.87 \times 10^3\text{Hz}$ the gravitational sag is calculated to be $\delta z = 1.1$ nm which is negligibly small. Therefore, the effect of gravitational sag on the trap confinement can be neglected.

Table 3. the analytical and numerical calculations using the input parameters reported in Table 1 for ^{87}Rb in the $F = +2$ and m=+2 state for two cases $B_{1z} = 0$ and $B_{1z} \neq 0$

Parameters	Definition	Analytical $B_{1z} = 0$	Analytical $B_{1z} \neq 0$	Numerical
B_{min} (G)	Minimum of B	2.730	2.730	2.729
y_{min} (μm)	y coordinate of B_{min}	0.250	0.009	0.009
z_{min} (μm)	z coordinate of B_{min}	1.212	0.750	0.750
$\frac{\partial^2 B}{\partial y^2}(\frac{G}{cm^2})$	Curvature of B along y-axis	6.999×10^7	2.321×10^{10}	2.324×10^{10}
$\frac{\partial^2 B}{\partial z^2}(\frac{G}{cm^2})$	Curvature of B along z-axis	6.999×10^7	2.321×10^{10}	2.324×10^{10}
ΔB^y (G)	B barrier height along y-axis	0.035	5.734	5.742
ΔB^z (G)	B barrier height along z-axis	0.009	2.118	2.134
$\Delta U^y/k_B$ (μK)	Potential energy barrier height along y-axis	2.366	385.189	385.709
$\Delta U^z/k_B$ (μK)	Potential energy barrier height along z-axis	0.594	142.256	143.343
$\omega_y/2\pi$ (kHz)	Trap frequency along y-axis	10.676	194.393	194.636
$\omega_z/2\pi$ (kHz)	Trap frequency along z-axis	10.676	194.393	194.449

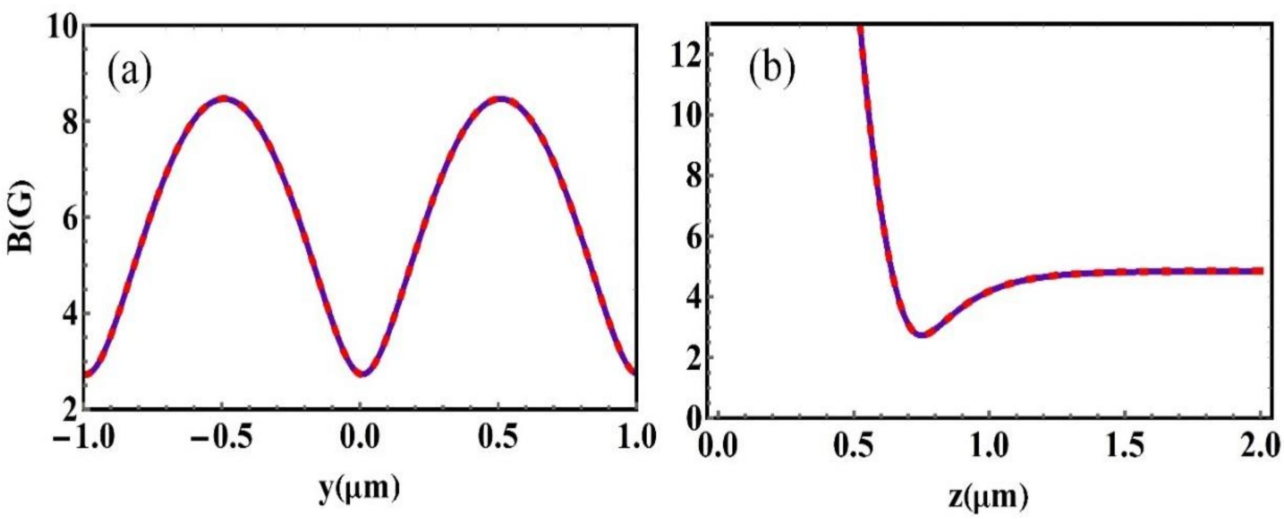

Figure 8. Comparison of the analytical (solid line) and numerical (dashed line) results for the absolute value of the magnetic field using input parameters reported in Tables (1) and (2) for ^{87}Rb in the $F = +2$ and m=+2 state (a) the y direction (b) the z direction

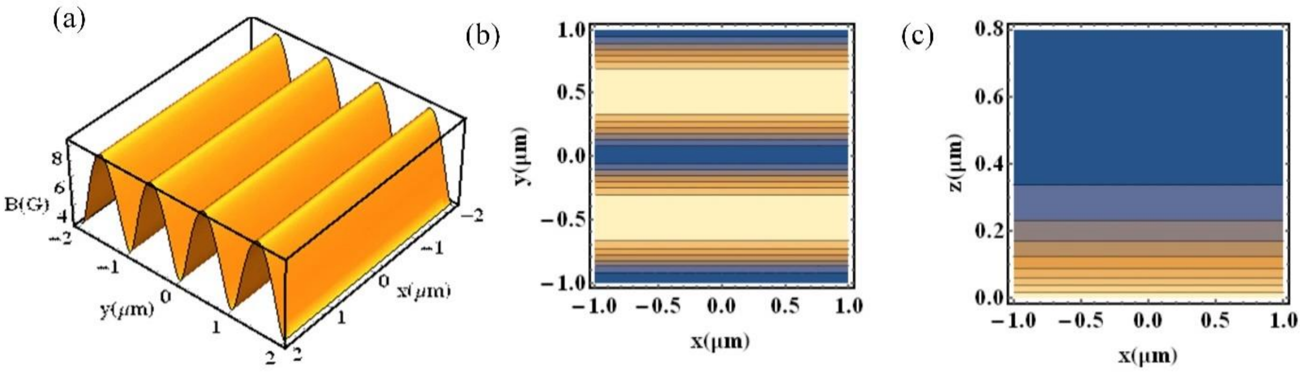

Figure 9. (a) 3D plot of the non-zero magnetic field minimum (b) contour plot of the magnetic field for $z = z_{min}$ (c) contour plot of B for $y = y_{min}$

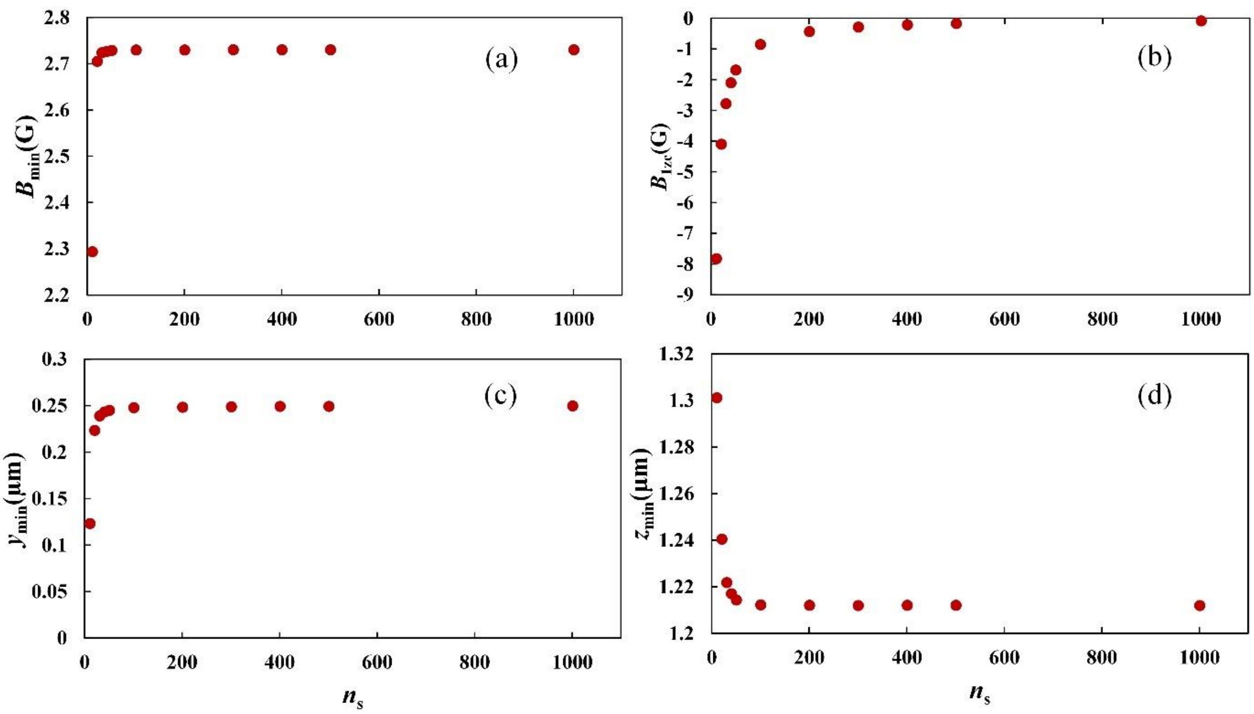

Figure 10. Variation of the trap parameters as a function of the lattice size n_s (a) B_{min} (b) B_{1zc} (c) y_{min} (d) z_{min}

Table 4. Numerical values of different parameters for selected lattice sizes

n_s	B_{1zc} (G)	y_{min} (μm)	z_{min} (μm)	B_{min} (G)	$\omega_y/2\pi$ (kHz)	$\omega_z/2\pi$ (kHz)	$\Delta U^y/k_B$ (μK)	$\Delta U^z/k_B$ (μK)
31	-2.777	0.239	1.222	2.724	10.416	9.424	2.108	0.356
51	-1.688	0.245	1.214	2.728	10.565	10.379	2.304	0.522
201	-0.428	0.248	1.212	2.729	10.671	10.676	2.366	0.593
401	-0.215	0.249	1.212	2.730	10.681	10.672	2.366	0.594
1001	-0.086	0.249	1.212	2.730	10.672	10.675	2.367	0.595

4. Conclusion

In this work, we have proposed a permanent magnetic waveguide array produced by high quality magneto-optical film FePt in the presence of three bias magnetic field components B_{1x}, B_{1y} and B_{1z} for trapping ^{87}Rb atoms in the low magnetic field-seeking state $|F = +2, m_F = +2\rangle$. We have presented our results using two analytical and numerical approaches and compared them. For the first time, we have derived the analytical dependence of various trap parameters, including the locations of the magnetic field minima, the curvatures of the magnetic field, trap frequencies, and the trap depths along the *y* and *z* directions on B_{1x}, B_{1y}, and B_{1z}. We have also, investigated the effect of the bias magnetic field component in the *z* direction on the magnetic microtrap properties. Moreover, we have demonstrated that the derived analytical expressions reduce to the equations reported in Ref. [19] for $B_{1z} = 0$. Furthermore, we have compared the variations of the magnetic field minima locations $(y_{\min}, z_{\min})$, the trap frequencies (ω_y, ω_z) and the trap depths $(\varDelta U^y, \varDelta U^z)$ as a function of B_{1x} and B_{1y} in the presence of $B_{1z} \neq 0$ rather than $B_{1z} = 0$ in order to show the effect of B_{1z}. Therefore, the analysis of the results indicates that B_{1z} is an effective parameter for controlling the trap frequencies and the potential barrier height. This component provides more control over the trap depth and contributes to the generation of deeper permanent magnetic microtraps. In the numerical approach, the trap parameters have been calculated using the Radia software package, and the influence of $B_{1z} \neq 0$ compared with $B_{1z} = 0$ was investigated, demonstrating improved control over the trap parameters. Furthermore, we have presented analytical and numerical plots to compare the results and demonstrated good agreement. For further analysis, we have considered several lattice sizes and investigated the trends of different trap parameters. We have concluded that increasing the lattice size n_s leads to a decrease in the compensating magnetic field component toward zero and causes the magnetic field minima to approach the analytical results obtained for an infinite lattice. Based on our analytical and numerical calculations, we have shown that increasing B_{1z} enhances the trap frequencies and trap depths, thereby providing improved control over the magnetic microtraps.

References

[1] J. Reichel, V. Vuletic, Atom chips (John Wiley & Sons, 2011).

[2] W. Hänsel, P. Hommelhoff, T. Hänsch, J. Reichel, Bose–Einstein condensation on a microelectronic chip, nature 413 (2001) 498-501.

[3] H. Ott, J. Fortagh, G. Schlotterbeck, A. Grossmann, C. Zimmermann, Bose-Einstein Condensation in a surface micro trap, arXiv preprint cond-mat/0109322 (2001).

[4] R. Folman, Material science for quantum computing with atom chips, Quantum Information Processing 10 (2011) 995-1036.

[5] E. Hinds, I. Hughes, Magnetic atom optics: mirrors, guides, traps, and chips for atoms, Journal of Physics D: Applied Physics 32 (1999) R119.

[6] R. Folman, P. Krüger, D. Cassettari, B. Hessmo, T. Maier, J. Schmiedmayer, Controlling cold atoms using nanofabricated surfaces: Atom chips, Physical review letters 84 (2000) 4749.

[7] V. Leung, D. Pijn, H. Schlatter, L. Torralbo-Campo, A. La Rooij, G. Mulder, J. Naber, M. Soudijn, A. Tauschinsky, C. Abarbanel, Magnetic-film atom chip with 10 μm period lattices of microtraps for quantum

information science with Rydberg atoms, Review of Scientific Instruments 85 (2014).

[8] I. Bloch, Ultracold quantum gases in optical lattices, Nature physics 1 (2005) 23-30.

[9] D. Jaksch, C. Bruder, J.I. Cirac, C.W. Gardiner, P. Zoller, Cold bosonic atoms in optical lattices, Physical review letters 81 (1998) 3108.

[10] I. Bloch, Quantum gases in optical lattices, Physics World 17 (2004) 25.

[11] F. Schäfer, T. Fukuhara, S. Sugawa, Y. Takasu, Y. Takahashi, Tools for quantum simulation with ultracold atoms in optical lattices, Nature Reviews Physics 2 (2020) 411-425.

[12] M. Greiner, O. Mandel, T. Esslinger, T.W. Hänsch, I. Bloch, Quantum phase transition from a superfluid to a Mott insulator in a gas of ultracold atoms, nature 415 (2002) 39-44.

[13] T. Calarco, U. Dorner, P.S. Julienne, C.J. Williams, P. Zoller, Quantum computations with atoms in optical lattices: Marker qubits and molecular interactions, Physical Review A—Atomic, Molecular, and Optical Physics 70 (2004) 012306.

[14] C. Gross, I. Bloch, Quantum simulations with ultracold atoms in optical lattices, Science 357 (2017) 995-1001.

[15] H. Katori, Optical lattice clocks and quantum metrology, Nature Photonics 5 (2011) 203-210.

[16] V. Singh, V. Tiwari, A. Chaudhary, R. Shukla, C. Mukherjee, S. Mishra, Development and characterization of atom chip for magnetic trapping of atoms, Journal of Applied Physics 133 (2023).

[17] A. Haase, D. Cassettari, B. Hessmo, J. Schmiedmayer, Trapping neutral atoms with a wire, Physical Review A 64 (2001) 043405.

[18] J. Denschlag, D. Cassettari, A. Chenet, S. Schneider, J. Schmiedmayer, A neutral atom and a wire: towards mesoscopic atom optics, Applied Physics B 69 (1999) 291-301.

[19] S. Ghanbari, T.D. Kieu, A. Sidorov, P. Hannaford, Permanent magnetic lattices for ultracold atoms and quantum degenerate gases, Journal of Physics B: Atomic, Molecular and Optical Physics 39 (2006) 847.

[20] S. Ghanbari, T.D. Kieu, P. Hannaford, A class of permanent magnetic lattices for ultracold atoms, Journal of Physics B: Atomic, Molecular and Optical Physics 40 (2007) 1283.

[21] S. Ghanbari, A. Abdalrahman, A. Sidorov, P. Hannaford, Analysis of a simple square magnetic lattice for ultracold atoms, Journal of Physics B: Atomic, Molecular and Optical Physics 47 (2014) 115301.

[22] J. Fortágh, C. Zimmermann, Magnetic microtraps for ultracold atoms, Reviews of Modern Physics 79 (2007) 235.

[23] P. Karimi, S. Ghanbari, Analytic expressions for a 2D permanent magnetic lattice with a 3D bias magnetic field for ultracold atoms, Journal of Low Temperature Physics 192 (2018) 212-223.

[24] S. Ghanbari, 3D permanent magnetic lattices for ultracold atoms, Physica Scripta 98 (2023) 105412.

[25] A. Mohammadi, S. Ghanbari, A. Pariz, A two-dimensional permanent magnetic lattice for ultracold atoms, Physica Scripta 88

(2013) 015601.

[26] P. Surendran, S. Jose, Y. Wang, I. Herrera, H. Hu, X. Liu, S. Whitlock, R. McLean, A. Sidorov, P. Hannaford, Radio-frequency spectroscopy of a linear array of Bose-Einstein condensates in a magnetic lattice, Physical Review A 91 (2015) 023605.

[27] M. Singh, R. McLean, A. Sidorov, P. Hannaford, Dynamics of reflection of ultracold atoms from a periodic one-dimensional magnetic lattice potential, Physical Review A—Atomic, Molecular, and Optical Physics 79 (2009) 053407.

[28] R. Schmied, D. Leibfried, R.J. Spreeuw, S. Whitlock, Optimized magnetic lattices for ultracold atomic ensembles, New Journal of Physics 12 (2010) 103029.

[29] Y. Wang, T. Tran, P. Surendran, I. Herrera, A. Balcytis, D. Nissen, M. Albrecht, A. Sidorov, P. Hannaford, Trapping ultracold atoms in a sub-micron-period triangular magnetic lattice, Physical Review A 96 (2017) 013630.

[30] A. La Rooij, S. Couet, M. Van Der Krogt, A. Vantomme, K. Temst, R. Spreeuw, Deposition and patterning of magnetic atom trap lattices in FePt films with periods down to 200 nm, Journal of Applied Physics 124 (2018).

[31] P. Karimi, S. Ghanbari, F. Rezaei, A comparison of trapping the rubidium atoms in optical and magnetic lattices, Physica Scripta 96 (2021) 065403.

[32] S. Ghanbari, P. Blair Blakie, P. Hannaford, T.D. Kieu, Superfluid to Mott insulator quantum phase transition in a 2D permanent magnetic lattice, The European Physical Journal B 70 (2009) 305-310.

[33] X.-Y. Dong, F. Pollmann, X.-F. Zhang, Machine learning of quantum phase transitions, Physical Review B 99 (2019) 121104.

[34] H. Saito, Solving the Bose–Hubbard model with machine learning, Journal of the Physical Society of Japan 86 (2017) 093001.

[35] B.S. Rem, N. Käming, M. Tarnowski, L. Asteria, N. Fläschner, C. Becker, K. Sengstock, C. Weitenberg, Identifying quantum phase transitions using artificial neural networks on experimental data, Nature physics 15 (2019) 917-920.

[36] P. Karimi, M.-Y. Hosseini Varzaqani, S. Ghanbari, Machine learning and deep learning algorithms for prediction of different parameters of a 2D permanent magnetic lattice, Journal of Applied Physics 137 (2025).

[37] J. Reichel, Microchip traps and Bose–Einstein condensation, Applied Physics B 74 (2002) 469-487.

[38] Y.-j. Lin, I. Teper, C. Chin, V. Vuletic, Impact of the Casimir-Polder potential and Johnson noise on Bose-Einstein condensate stability near surfaces, arXiv preprint cond-mat/0308457 (2003).

[39] V.Y. Leung, A. Tauschinsky, N. Van Druten, R.J. Spreeuw, Microtrap arrays on magnetic film atom chips for quantum information science, Quantum Information Processing 10 (2011) 955.

[40] S. Scheel, P.-K. Rekdal, P.L. Knight, E.A. Hinds, Atomic spin decoherence near conducting and superconducting films, Physical Review A—Atomic, Molecular, and Optical Physics 72 (2005) 042901.

[41] Y. Dai, Y. Zhao, L. Ma, M. Tang, X. Qiu, Y. Liu, Z. Yuan, S. Zhou, Fourfold anisotropic magnetoresistance of L 1 0 FePt due to relaxation time anisotropy, Physical review letters 128 (2022) 247202.

[42] S. Whitlock, B. Hall, T. Roach, R. Anderson, M. Volk, P. Hannaford, A. Sidorov, Effect of magnetization inhomogeneity on magnetic microtraps for atoms, Physical Review A—Atomic, Molecular, and Optical Physics 75 (2007) 043602.

[43] J.F. Sherson, S.J. Park, P.L. Pedersen, N. Winter, M. Gajdacz, S. Mai, J. Arlt, The pump–probe coupling of matter wave packets to remote lattice states, New Journal of Physics 14 (2012) 083013.